Biophysical Journal Volume 104 February 2013 575–584

Amphipathic Lipid Packing Sensor Motifs: Probing Bilayer Defects with Hydrophobic Residues

Stefano Vanni,[†] Lydie Vamparys,[‡§¶] Romain Gautier,[†] Guillaume Drin,[†] Catherine Etchebest,[‡§¶] Patrick F. J. Fuchs,[‡§¶] and Bruno Antonny[†*]

[†]Institut de Pharmacologie Moléculaire et Cellulaire, Université de Nice Sophia-Antipolis and Centre National de la Recherche Scientifique, Unité Mixte de Recherche 7275, Valbonne, France; [‡]Institut National de la Santé et de la Recherche Médicale, U665, Paris, France; [§]Université Paris Diderot, Sorbonne Paris Cité, Unité Mixte de Recherche S665, Paris, France; and [¶]Institut National de la Transfusion Sanguine, Paris, France

ABSTRACT Sensing membrane curvature allows fine-tuning of complex reactions that occur at the surface of membrane-bound organelles. One of the most sensitive membrane curvature sensors, the Amphipathic Lipid Packing Sensor (ALPS) motif, does not seem to recognize the curved surface geometry of membranes per se; rather, it recognizes defects in lipid packing that arise from membrane bending. In a companion paper, we show that these defects can be mimicked by introducing conical lipids in a flat lipid bilayer, in agreement with experimental observations. Here, we use molecular-dynamics (MD) simulations to characterize ALPS binding to such lipid bilayers. The ALPS motif recognizes lipid-packing defects by a conserved mechanism: peptide partitioning is driven by the insertion of hydrophobic residues into large packing defects that are preformed in the bilayer. This insertion induces only minor modifications in the statistical distribution of the free packing defects. ALPS insertion is severely hampered when monounsaturated lipids are replaced by saturated lipids, leading to a decrease in packing defects. We propose that the hypersensitivity of ALPS motifs to lipid packing defects results from the repetitive use of hydrophobic insertions along the monotonous ALPS sequence.

INTRODUCTION

In early reconstitution experiments on liposomes, it was observed that the activity of the peripheral protein Arf GTPase-Activating Protein 1 (ArfGAP1) increased >2 orders of magnitude when conical lipids were introduced at the expense of cylindrical lipids in the bilayer (1). Later, an effect of similar amplitude was observed when the lipid composition was kept constant while the liposome radius was decreased from 150 to 30 nm (2). These two observations led to a model in which ArfGAP1 senses the packing defects between lipid molecules that arise from the mismatch between the actual curvature of the membrane and the lipid geometry.

Since then, this model has gained more interest. First, membrane curvature is recognized as an efficient index to control several biochemical reactions on membrane surfaces in space and time (3–8). In the case of ArfGAP1, its hypersensitivity to membrane curvature helps to organize two reactions: the assembly-disassembly cycle of the Coat Protein complex I (COPI) coat, a complex that shapes Golgi membranes into small transport vesicles, and the attachment of such vesicles by long tether proteins (2,9). Second, the motif by which ArfGAP1 recognizes membrane curvature has not only been identified (10,11) but has also been found in proteins with different functions, such as membrane tethers, nucleoporins, and lipid transporters (11–15). This motif is called the Amphipathic Lipid Packing Sensor (ALPS) motif.

ALPS motifs are sequences of 20–40 amino acids that, despite weak sequence identity, share similar physicochemical features (10,11). They contain hydrophobic residues that are regularly distributed every three or four residues, with a marked preference for bulky ones (e.g., Phe, Leu, and Trp). In between, small polar residues, notably Gly, Ser and Thr, are abundant, whereas charged residues are rare if not absent. ALPS motifs are intrinsically soluble but bind efficiently to liposomes that contain conical lipids (i.e., dioleoylglycerol) or display a highly positive curvature. Circular dichroism (CD) spectroscopy has shown that membrane adsorption of ALPS is accompanied by its folding into an α-helix (10,11,16), and molecular-dynamics (MD) simulations performed on the ALPS motif of ArfGAP1 in its membrane-embedded helical conformation suggested that its secondary structure is less stable than traditional amphipathic helices (17). Nevertheless, the molecular details of the interaction between ALPS motifs and biological membranes remain elusive because of the dual difficulty of performing structural studies on an intrinsically unfolded sequence and in a membrane environment. In particular, we still lack a thorough description of peptide partitioning into membranes, as well as a molecular understanding of how the specific amino acid composition of the peptide gives rise to its peculiar function as a curvature sensor.

The current model for sensing of membrane curvature by ALPS motifs posits that bulky hydrophobic residues serve as probes to detect the defects in lipid packing that arise from membrane bending (4,10,11,17). This mode of

Submitted June 27, 2012, and accepted for publication November 16, 2012.

*Correspondence: antonny@ipmc.cnrs.fr

Editor: Scott Feller.

0006-3495/13/02/0575/10 $2.00

http://dx.doi.org/10.1016/j.bpj.2012.11.3837

membrane curvature recognition, which is based solely on the hydrophobic effect, seems very different from that of well-folded domains such as BAR, which recognize membrane curvature via a complementary shape between their concave basic surface and convex acidic membranes (3,18). More generally, defects in lipid packing can be an asset for the adsorption of several peripheral proteins (e.g., α-synuclein), as well as for the functioning of transmembrane proteins (19–21).

To understand the hypersensitivity of the ALPS motif to membrane curvature and lipid geometry, it is necessary to address the differences, at the molecular level, between membranes that are abundant or scarce in packing defects. In a pioneering study, Voth and colleagues (22) characterized the packing defect distribution in anionic lipid bilayers of different curvatures by analyzing their accessible surface area (ASA). The size distribution of packing defects depends nontrivially on the curvature, and falls off exponentially with a characteristic constant that depends on curvature. In a companion study, we performed the same analysis on bilayers that contain lipids with different numbers of monounsaturated acyl chains and with or without the conical lipid dioleoylglycerol (23). Remarkably, using either the ASA approach or a new method based on Cartesian coordinates, we obtained a similar result: the size distribution of packing defects showed an exponential decay that depends on the number of monounsaturated acyl chains or on the introduction of conical lipids (23). Thus, inducing positive curvature and introducing conical lipids in a flat bilayer are two alternative ways to increase the occurrence of large lipid packing defects.

In this work, we explored the specific mechanism that couples the adsorption of ALPS motifs on the bilayer surface to lipid packing defects. We conducted MD simulations of the binding of the ALPS motifs of ArfGAP1 and GMAP210 to a lipid bilayer that is rich in packing defects. By simultaneously monitoring the interaction of the peptide with the bilayer and the localization and size of packing defects, we were able to show that the ALPS motif partitions in the bilayer via the insertion of hydrophobic residues into large preexisting packing defects that can be thought of as dynamical binding pockets for the inserting residues. The repetitive use of this elementary mode of membrane insertion along the monotonous ALPS sequence may explain the hypersensitivity shown by ALPS motifs to positively curved membranes.

MATERIALS AND METHODS

MD simulations

Two peptides were studied in this work. The first one was the first ALPS motif of ArfGAP1 (amino acids 197–231, sequence DDFLNSAMSSL YSGWSSFTTGASKFASAAKEGATK) (10,16,17). The N-and C- termini were acylated and aminated, respectively. Amino acids were numbered from 2 to 36, in agreement with previous literature (17). Thus, F26 in the peptide corresponds to F222 in ArfGAP1. The second peptide was the ALPS motif of GMAP210 (amino acids 1–38, sequence MSSWLGG LGSGLGQSLGQVGGSLASLTGQISNFTKDML). To faithfully model the peptide that has been studied experimentally (11), the N- and C-termini were in their default protonation state.

The peptides were modeled as a complete α-helix and then solvated in a box of water of $5 \times 5 \times 5$ nm^3 with charge-neutralizing counterions using periodic boundary conditions. Several replicas of the system were run for 50 ns, and unfolding of the peptide into a molten-globule state was observed after ~10 ns in all simulations. For each system, one of the final structures was used as a starting point for the peptide-membrane simulations. The two lipid bilayers used in this study were a patch of 250 dimyristoylphosphatidylcholine (DMPC) lipids of area 9×9 nm^2 and a patch of 240 dioleoylphosphatidylcholine (DOPC) and 40 dioleoylglycerol (DOG) lipids (molar ratio 85:15) of area 9.5×9.5 nm^2. The two bilayers were equilibrated by performing 100 ns of MD in a water box containing Na^+ and Cl^- ions at physiological concentration (120 mM). The final bilayer structures were used to start the simulations with the peptide. All peptide-bilayer simulations were initiated by placing the unfolded peptide at a distance of 2.5 nm from the lipid bilayer. Water molecules that spatially overlapped with the peptide, as well as excess ions, were removed to keep the overall system charge at zero. Each replica (five for ArfGAP1 with DOPC/DOG, five for ArfGAP1 with DMPC, five for GMAP210 with DOPC/DOG, and five for GMAP210 with DMPC) was started from the same conformation by assigning different random velocities. On average, the total number of atoms was 65,000 in a box of $9.5 \times 9.5 \times 10$ nm^3. All replicas were run for 400 ns, with the exception of two MD runs of ArfGAP1 with DOPC/DOG and two MD runs of GMAP210 with DOPC/DOG that were run for 1 μs. The cumulative length of the aforementioned MD runs amounted to 10.4 μs.

All data collections and equilibration runs were performed using GROMACS 4 (24), and the all-atom OPLS force field (25) was used for the protein in combination (26) with the Berger model for PC lipids (27) and with the TIP3P model (28) for water molecules. For DOG, we used our previous model based on the Berger model (with a charge of -0.7 e on the hydroxyl) (17). Because OPLS-AA and Berger lipids have different 1-4 combination rules, the half-ϵ double-pairlist method was used to mix both force fields (26,29). Electrostatic interactions were calculated with the Ewald particle mesh method (30), with a real-space cutoff of 1 nm. Bonds lengths were constrained using the LINCS algorithm (31) and the integration time step was set to 2 fs. The system was coupled to a Bussi thermostat (32) and to a semiisotropic Parrinello-Rahman barostat (33) at a temperature of 300 K and a pressure of 1 atm. Additional simulations of 1–2 μs of the ALPS motif of ArfGAP1 in a DOPC/DOG (85:15) bilayer were carried out at higher temperatures and are described in the Supporting Material. In addition, MD simulations of a toluene molecule, analog to phenylalanine side chain (34), and of two model peptides representative of individual turns of ALPS motifs (amino acid sequence: SFLG and SLG) are described in the Supporting Material.

Packing defects were computed using the Cartesian method described in the companion article (23). Unless otherwise specified, the packing defects discussed in this study are geometrical packing defects, i.e., packing defects that extend below the glycerol level. By convention, we define the instantaneous glycerol level as the average value along the normal to the membrane plane of the *sn*-2 carbon atom of all lipid molecules (for each leaflet separately) at a given time.

Data analysis was done using GROMACS utilities, and molecular images were made with the use of Visual Molecular Dynamics (VMD) (35) and PyMol (36).

CD spectroscopy

The ArfGAP1[197-231] peptide, whose N- and C-termini were acylated and aminated, respectively, was purchased from Proteogenix (France). DOPC (1,2-dioleoyl-*sn*-glycero-3-phosphocholine) and DOG

(1-2-dioleoyl-*sn*-glycerol) were purchased from Avanti Polar Lipids (Alabaster, AL). The peptide was solubilized in 10 mM Tris pH 7.2, 120 mM NaCl buffer, and the concentration of stock solutions was carefully determined by absorbency at 280 nm ($\varepsilon = 6990\ M^{-1}.cm^{-1}$). To produce liposomes, dried films were prepared by evaporation of lipids in chloroform and resuspended in 10 mM Tris pH 7.2 and 120 mM NaCl. After five freeze-thawing cycles, the liposome suspension (10 mM lipids) was extruded through 0.2 μm polycarbonate filters. Alternatively, the suspension was sonicated with a titanium tip sonicator to obtain small liposomes. Titanium and lipid debris were removed by centrifugation at 100,000 *g* for 20 min. The hydrodynamic radius (R_H) of large and small liposomes was determined by dynamic light scattering in a Dyna Pro instrument. Liposomes were stored at room temperature and used within 2 days after preparation. The CD experiments were performed on a Jasco J-815 spectrometer at controlled temperature with a quartz cell of 0.05 cm path length. Each spectrum is the average of 10 scans recorded from 200 to 260 nm with a bandwidth of 1 nm, a step size of 0.5 nm, and a scan speed of 50 nm/min. Control spectra of buffer with or without liposomes were subtracted from the peptide spectra.

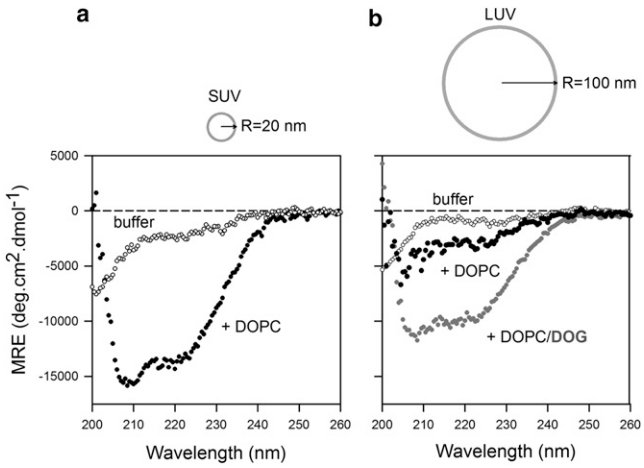

FIGURE 1 The ALPS motif of ArfGAP1 binds to large DOPC/DOG liposomes. (*a*) CD spectra of the ArfGAP1 (amino acids 197–231) peptide in the absence (*white dots*) or presence (*black dots*) of sonicated DOPC liposomes ($R_H = 16.6 \pm 8$ nm). (*b*) Spectra of the peptide alone (*white dots*) or in the presence of large DOPC ($R_H = 115 \pm 52$ nm; *black dots*) or DOPC/DOG liposomes (85/15 mol/mol, $R_H = 108 \pm 48$ nm; *gray dots*). All experiments were performed at 25°C in 10 mM Tris pH 7.2 and 120 mM NaCl buffer. Peptide concentration: 25 μM; lipid concentration: 5 mM.

RESULTS AND DISCUSSION

The ALPS motif of ArfGAP1 binds to DOPC/DOG bilayers via the insertion of large hydrophobic residues

According to several observations and models (37–41), amphipathic peptides bind to lipid bilayers in two steps: partitioning of the peptide from the solvent to the interfacial region of the bilayer, followed by folding into a partial or complete α-helix. Although the dynamic behavior of the ALPS motif of ArfGAP1 in its α-helical state when inserted into a lipid bilayer was recently reported (17), little is known about its partitioning mechanism at the molecular level. Previous experiments showed that ALPS binds to large liposomes containing conical lipids as efficiently as it does to small liposomes (1,2). We thus conducted CD experiments to check the secondary structure upon binding and to determine the optimal content of DOG for binding to large liposomes. These experiments indicated that a DOPC/DOG ratio of 85:15 is appropriate, because the ALPS peptide is capable of binding to large liposomes of such composition, but this capability is severely hampered when DOG is removed (Fig. 1).

To characterize the mechanism of ALPS motif partitioning into a model membrane, we thus performed MD simulations of the ALPS motif of ArfGAP1 in the presence of an explicit lipid bilayer. A total of five MD replicas (Table 1) for a cumulative length of 3.2 μs were performed starting from a conformation in which the peptide was unfolded and placed >2 nm away from the bilayer surface (see Materials and Methods). This choice was motivated by recent MD simulations that showed that amphipathic peptides in an initial random-coil structure form contacts with lipids more frequently than do folded peptides (42), and it was further justified by the a posteriori observation that the ALPS motif is able to sample multiple conformations before binding to the bilayer (Fig. S1). We also noted that the peptide could bind to the upper or lower leaflet (due to periodic conditions) independently of the initial configuration, which suggests that the results were not biased by the choice of the starting point.

The details of the binding mechanism are summarized in Table 1. In all replicas, the peptide started adsorbing to the lipid bilayer within the first 100 ns through the insertion of one hydrophobic residue below the glycerol group of the lipids. Of importance, and regardless of the residue that inserted, insertion was always irreversible, i.e., the residue never dissociated from the bilayer, but instead resided around the glycerol level for the remainder of the simulation (Fig. S2). In four out of five replicas, the residue that inserted first was phenylalanine 26 (F26), possibly as a consequence of its proximity to a lysine (K25), which may favor bilayer binding through electrostatic interactions with the lipid polar headgroups. In the fifth replica, the insertion proceeded through the simultaneous insertion, in very close spatial proximity, of leucine 12 (L12) and alanine 34 (A34) into the lipid bilayer. In two out of four replicas, insertion of F26 was followed by insertion of a distant residue, phenylalanine 4 (F4), which itself was accompanied by an almost simultaneous very shallow insertion of a nearby leucine (L5).

An example of the time evolution of peptide insertion is detailed in Fig. 2. The insertion of F26 took place after ~50 ns (Fig. 2 *a*) and was associated with a large decrease (~300 kJ/mol) in the Lennard-Jones (LJ) interaction between the peptide and the lipid bilayer (Fig. 2 *c*). The second event, insertion of F4, took place after 218 ns

TABLE 1 Insertion mechanism of the ALPS motif of ArfGAP1 in a DOPC/DOG (85:15) bilayer

		Insertion sequence						
		Insertion 1			Insertion 2			
MD run	MD length	Time (ns)	Amino acid	Defect size before insertion (nm^2)[a]	Time (ns)	Amino acid	Defect size before insertion (nm^2)[a]	Protein-bilayer LJ (kJ/mol)[b]
MD *a*	1 μs	59	F26	0.29	-	-	-	−295
MD *b*	1 μs	52	F26	0.75	437	F4	0.52	−591
MD *c*	400 ns	47	F26	0.23	218	F4	0.21	−552
MD *d*	400 ns	86	F26	0.21	-	-	-	−318
MD *e*	400 ns	103	L12	0.24	-	-	-	−442

[a]The defect size before insertion is the average value over the last nanosecond preceding insertion.
[b]The average protein-bilayer LJ energy is computed in the time window between 300 and 400 ns.

(Fig. 2 *b*) and was associated with a similar decrease in LJ interaction energy. In Fig. 2 *d*, the evolution of the backbone density of the peptide along the axis normal to the bilayer surface is plotted for consecutive time windows. Backbone insertion proceeded through two big jumps, at 40–80 and 200–240 ns time windows corresponding to F26 and F4 insertions, and was combined with smoother rearrangements of the backbone at the glycerol-phosphate interface. The conformation of the peptide in the bilayer after 280 ns is shown in Fig. 2 *e*.

Taken together, the various MD simulations indicate that the insertion of large hydrophobic residues is favored with respect to smaller ones (the ALPS motif of ArfGAP1 is also rich in alanines), suggesting that the DOPC/DOG bilayer used in our simulations displays a permissive structure that allows large residues to insert.

Large hydrophobic residues of ALPS insert into preexisting packing defects

Next, we wished to determine how ALPS partitioning is coupled to the packing structure of the lipid bilayer. To that end, we used a Cartesian-based approach that is explained in detail in the companion article (23). In short, we selected a plane that was perpendicular to the membrane normal and created a grid of 0.1 nm resolution. For each grid point, we scanned the normal of the membrane plane starting from the solvent and descending up to 0.1 nm below the

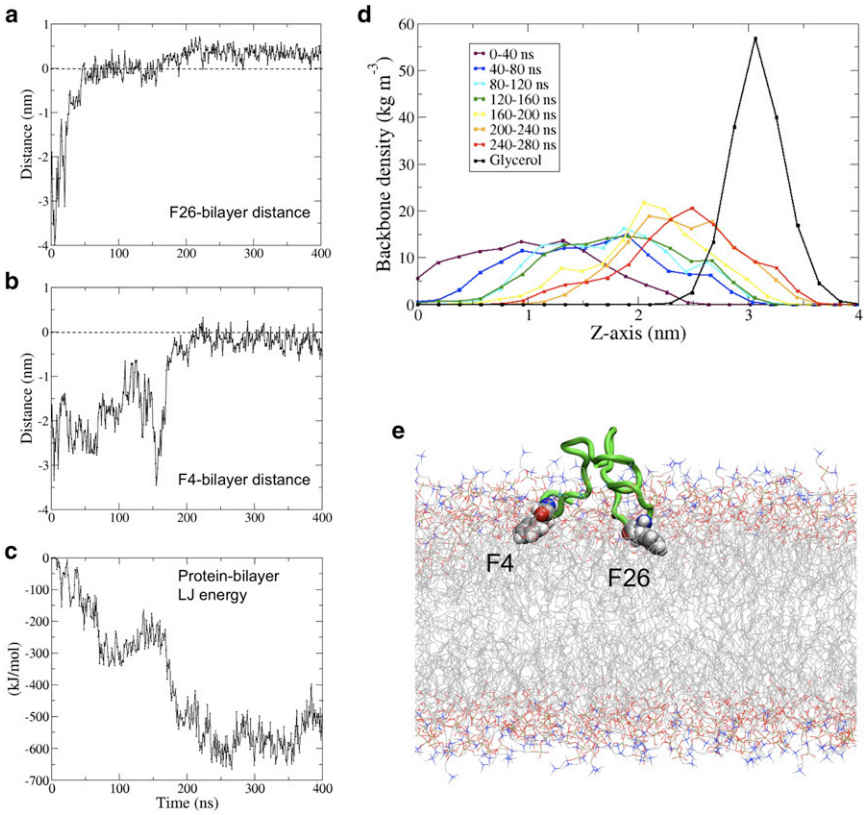

FIGURE 2 Insertion mechanism of the ALPS motif of ArfGAP1 in a DOPC/DOG bilayer. (*a*) Time evolution of the distance between the center of mass of residue F26 and the average glycerol level of lipid molecules. (*b*) Time evolution of the distance between the center of mass of residue F4 and the average glycerol level of lipid molecules. (*c*) Time evolution of the LJ energy between the protein and the lipid molecules. (*d*) Averaged time evolution of protein backbone density along the normal to the bilayer plane. (*e*) MD snapshot (t = 280 ns) of the ALPS motif of ArfGAP1 inserted into a DOPC/DOG bilayer. The peptide is shown in green in cartoon representation and the inserting phenylalanine residues (F26 and F4) are shown in van der Waals (vdW) representation. All data shown are taken from MD run *c*.

glycerol level. If no lipid atom was met, we retained the grid point and defined it as a geometrical defect of size of 0.01 nm^2; in all other cases the grid point was discarded. Adjacent elementary defects were then merged, resulting in defects of various sizes.

Fig. 3 shows a snapshot of the MD simulations, where the packing defects of a DOPC/DOG bilayer are represented (in *blue*) together with the ALPS motif. As expected, the regions where the peptide inserted colocalized with large packing defects. Interestingly, no correlation between the region of ALPS binding and the localization of DOG lipids was observed (the colocalization between packing defects and DOG lipids was constantly below 5% before and after peptide insertion), in agreement with the finding that DOG lipids do not generate packing defects in their close surroundings, but rather change macroscopic bilayer properties (23).

The overlap between peptide insertion and large packing defects could be interpreted in two ways. In the first scenario, the lipids reorient themselves after peptide insertion to accommodate the bulky Phe side chain. Alternatively, the peptide binds directly to one of the preformed transient cavities. To distinguish between these two possibilities, we studied the time correlation between phenylalanine insertion and the appearance of lipid packing defects.

Fig. 4 reports the dynamics of F26 insertion in a representative MD simulation. The red line represents the distance

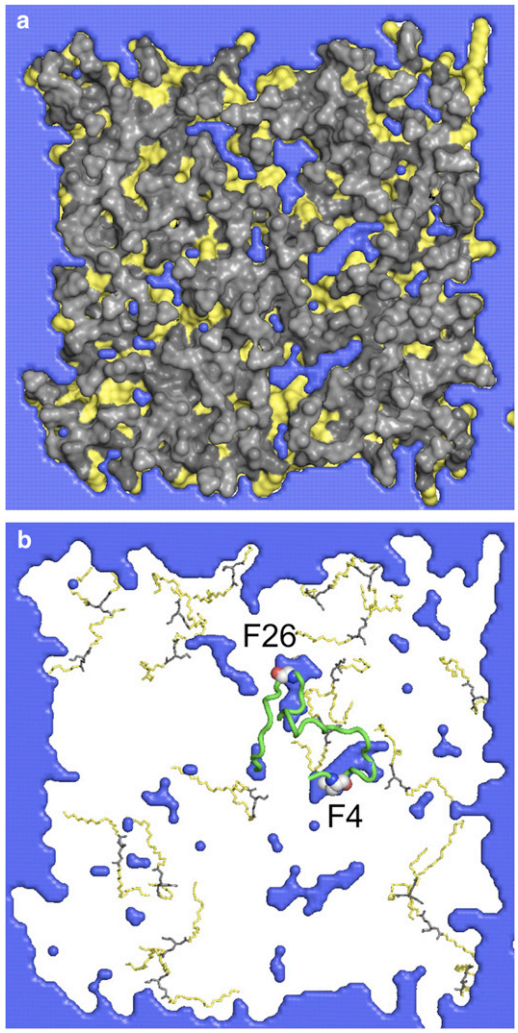

FIGURE 3 Colocalization between lipid packing defects and peptide insertion. (*a*) Top view of lipid molecules and packing defects in a representative snapshot from MD simulations of the ALPS motif of ArfGAP1 with a DOPC/DOG bilayer. Lipids are shown in surface representation with acyl chains in yellow and polar heads in gray. Packing defects are depicted in blue. The peptide is not shown. The apparent defects at the contour of the lipid bilayer are shown for clarity but are not considered as packing defects in the analysis. (*b*) Colocalization between the ALPS motif of ArfGAP1 and lipid packing defects. The peptide is shown in green in cartoon representation and the inserting phenylalanine residues (F26 and F4) are shown in vdW representation. DOG molecules are shown in licorice representation.

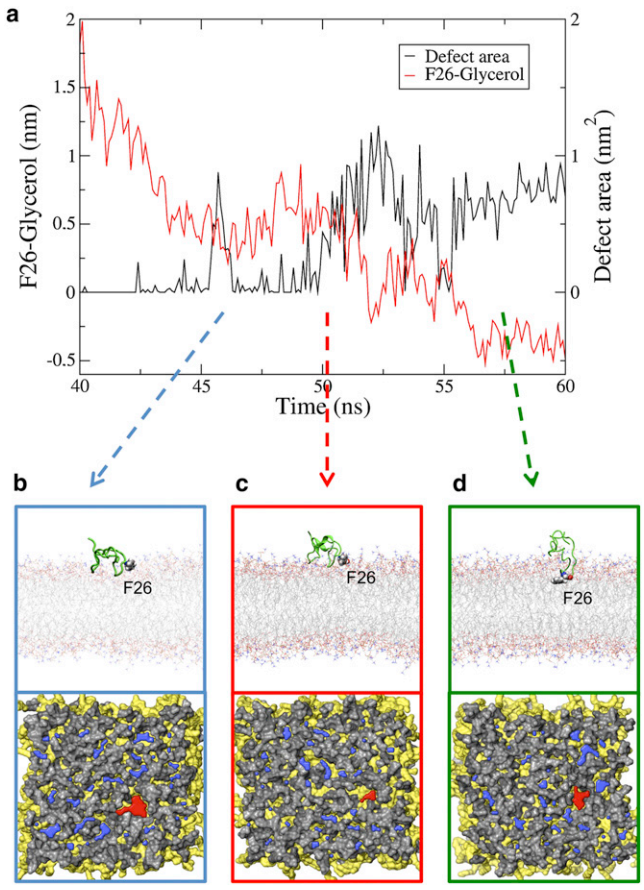

FIGURE 4 Role of packing defects in the insertion mechanism of hydrophobic residues. (*a*) Time evolution of the distance computed along the normal to the lipid bilayer between the center of mass of F26 and the average coordinate of the glycerol atoms (*red*) and time evolution of the size of the packing defect with the same coordinates in the membrane plane as F26 (*black*). (*b–d*) Upper panel: side view of the protein and lipid molecules in the proximity of a lipid packing defect at different times. In *b*, insertion does not take place; in *c* the residue is about to insert below the glycerol level; and in *d* the residue is fully inserted. Lower panel: localization of packing defects in the corresponding snapshots. The packing defect that is localized in close proximity to F26 is depicted in red.

between the center of mass of the inserting residue and the average coordinate of the glycerol, and the black line corresponds to the size of the geometrical packing defect that has the same coordinates in the membrane plane as the inserting residue (Fig. 4 *a*). F26 approached the lipid bilayer surface from the bulk solvent quite rapidly, taking ~4 ns to move from 2 nm to 0.5 nm above the glycerol level. At $t =$ 46 ns, a large geometrical packing defect (maximum size of 0.9 nm^2) formed underneath F26 (Fig. 4 *b*). Although F26 was in close proximity to this defect, it did not insert, and the defect disappeared after 2 ns. Five nanoseconds later, another large defect formed (Fig. 4 *c*). This time, F26 was capable of inserting and resided there for the remainder of the simulation (Fig. 4 *d*).

We performed the same analysis for all simulations, defining insertion as the first snapshot for which the center of mass of the residue was below the average glycerol level and resided there for at least 1 ns. Strikingly, in all cases a geometrical packing defect extending for at least 0.1 nm below the glycerol was already present before insertion (Table 1). After insertion, the size of the defect remained approximately unchanged for the remainder of the simulation, and no dissociation of the inserting residues was observed. The desolvation cost of the polar heads associated with the hydrophobic insertion may explain why the residue does not insert each time a defect is formed (it also justifies our choice to wait 1 ns for defining an insertion event). Interestingly, the size of these geometrical defects was always >0.2 nm^2 (Table 1), a dimension that is compatible with the size of the aromatic side chain of phenylalanine.

To further improve the statistics of the colocalization between hydrophobic insertions and preexisting lipid packing defects, we performed additional MD simulations of toluene molecules, analog to phenylalanine side chain (34), and of model peptides representative of conserved individual turns of ALPS motifs (amino acid sequence: SFLG and SLG). Whereas the insertion of toluene into DOPC/DOG bilayers (lacking any polar moiety) did not correlate with preexisting packing defects (Fig. S3), the insertions of the two minimal ALPS peptides correlated perfectly with preexisting packing defects (Fig. S4). Thus, hydrophobic side chains in an otherwise flexible and polar sequence can act as probes to detect packing defects in lipid bilayers.

Peptide insertion induces only minor modifications of the statistical distribution of free packing defects

Next, we assessed the effect of peptide insertion on the packing defect structure of the bilayer. For this, we computed the size distribution of packing defects of the DOPC/DOG bilayer after F26 insertion and compared it with the same distribution for a pure DOPC/DOG bilayer (Fig. 5). We initially performed this analysis on the entire bilayer surface by counting all defects, whether they were covered or not by the ALPS peptide.

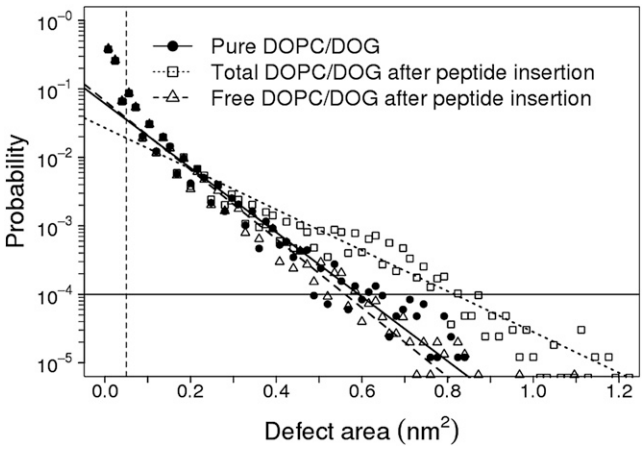

FIGURE 5 Effect of peptide insertion on the size distribution of lipid packing defects. Histograms and exponential fit of defect areas in different conditions: pure DOPC/DOG bilayer (*black dots*) and DOPC/DOG bilayer after peptide insertion (*white squares* and *white triangles*). White squares: all packing defects in the leaflet where insertion takes place; white triangles: packing defects in the leaflet where insertion takes place after removal of defects that are occupied by the inserting peptide.

Binding of the peptide to the bilayer significantly increased the occurrence of large packing defects compared with small ones. The difference with respect to a pure DOPC/DOG bilayer was significant for defects > 0.3 nm^2. This size is comparable to the value observed for the preexisting defects into which hydrophobic residues inserted (Table 1).

Next we refined the surface analysis by distinguishing, in the leaflet where insertion takes place, the defects underneath the ALPS motif from those remaining in the naked part of the bilayer. From this analysis, we made two important observations. First, the very large defects were directly underneath the ALPS motif, suggesting that hydrophobic residues, once inserted, stabilize large packing defects by filling them. This stabilization is a corollary of the fact that hydrophobic insertions are irreversible within our timescale. Second, and importantly, the surface that was not in contact with ALPS displayed a packing defect probability distribution very close to that observed before insertion. Therefore, should a second insertion occur, it would be facing a similar membrane structure as the first one. This picture is suggestive of an iterative process whereby the packing structure of the bilayer can be probed n times thanks to the repetitive feature of the ALPS sequence.

Binding of ALPS motifs to the lipid bilayer is an iterative process

Within the timescale of our simulations (≈ 1 μs) at room temperature, partitioning of the ALPS motif of ArfGAP1 into the bilayer was not complete, because only one or two hydrophobic insertions could be observed.

To circumvent this and to speed up the partitioning process, we first performed MD simulations at higher temperatures (see Supporting Material for details). As expected, we observed more insertions compared with MD performed at room temperature. Depending on the simulation, the sequence order of the insertions varied, suggesting a random process (Table S1). Interestingly, the partitioning process seemed to involve different steps: 1), adsorption of many hydrophobic residues while the peptide was still in a molten globule state; 2), peptide extension along the membrane surface; and 3), transient formation of helical segments on the N- and C-termini of the peptide.

The results of a simulation performed at nonphysiological temperature must be interpreted with caution. Using CD spectroscopy, we noticed a gradual decrease in the α-helicity of the ALPS peptide when it was incubated with DOPC/DOG (85:15) liposomes at increasing temperature (Fig. S5). In addition, a geometrical analysis of the lipid packing structure shows that increasing temperature induces a general increase in the size and number of lipid packing defects (Fig. S6), although both the exponential distribution and the relative difference between different lipid compositions remain valid. Notwithstanding these limitations, simulations at high temperature are suggestive of an iterative process whereby the ALPS motif of ArfGAP1 senses n times the packing structure of the bilayer through multiple hydrophobic insertions.

As an independent test of the iterative insertion model, we next performed room-temperature MD simulations of another ALPS motif that displays high sensitivity to membrane curvature, that of GMAP210, a tethering factor that regulates vesicular transport in the Golgi apparatus (9). The choice of this motif was motivated by two main observations: 1) it has a large number of bulky hydrophobic residues that can potentially insert into bilayer defects; and 2), it contains a high number of glycines that should confer higher flexibility to the motif.

Five independent MD simulations of the ALPS motif of GMAP210 in the presence of DOPC/DOG bilayer confirmed that the peptide binds to the bilayer through repeated irreversible hydrophobic insertions into preformed packing defects in a stochastic manner (Table 2). Specifically, in two 1 μs-long MD runs, we observed 10 and seven successive insertions (Table 2 and Fig. 6), respectively, of large hydrophobic residues (Phe, Trp, Leu, Ile, and Met), and insertion of nearby residues was accompanied by the formation of transient α-helical turns.

ALPS motifs prefer lipid bilayers with a higher density of large packing defects

Because ALPS motifs seem to partition into membranes through successive insertions of hydrophobic residues in distinct packing defects, the availability of large packing defects in a limited portion of the bilayer should determine the speed of insertion.

To test this hypothesis, we simulated the ALPS motifs of ArfGAP1 and GMAP210 in the presence of a DMPC bilayer, a lipid composition that, given the full saturation of the acyl chains, is very scarce in packing defects (Fig. 7 *a*) (23). To compare the results with the simulations performed in the presence of the DOPC/DOG bilayer, we adopted an identical

TABLE 2 Insertion mechanism of the ALPS motif of ArfGAP1 and GMAP210 in different lipid bilayers

Peptide	Lipid bilayer	MD run	MD length	Sequence of insertions (time)[a]	Insertions before 400 ns
ArfGAP1	DOPC DOG	1	1 μs	F26 (59 ns)	7
		2	1 μs	F26 (52 ns); F4(437 ns); L5 (440 ns); M9 (532 ns)	
		3	400 ns	F26 (47 ns), F4 (218 ns); L5 (220 ns)	
		4	400 ns	F26 (86 ns)	
		5	400 ns	L12 (103 ns)	
ArfGAP1	DMPC	1	400 ns	F19 (196 ns); W16 (360 ns)	4
		2	400 ns	-	
		3	400 ns	-	
		4	400 ns	F26 (133 ns)	
		5	400 ns	F26 (218 ns)	
GMAP210	DOPC DOG	1	1 μs	F33 (18 ns); M1 (28 ns); L5 (112 ns); I30 (155 ns); L26 (224 ns); W4 (310 ns); M37 (430 ns); L16 (431 ns); L38 (459 ns) ; L8 (533 ns)	19
		2	1 μs	M1 (24 ns); W5 (122 ns); L5 (294 ns); L23 (736 ns); L12 (810 ns); L16 (833 ns); L8 (848 ns)	
		3	400 ns	L23 (19 ns); L26 (19 ns); I30 (20 ns)	
		4	400 ns	L8 (52 ns); L23 (165 ns); L26 (245 ns)	
		5	400 ns	W4 (49 ns); M1 (178 ns); L16 (329 ns); L26 (399 ns)	
GMAP210	DMPC	1	400 ns	-	8
		2	400 ns	L12 (53 ns); L8 (191 ns); L5 (194 ns)	
		3	400 ns	I30 (331 ns)	
		4	400 ns	L26 (64 ns)	
		5	400 ns	W4 (50 ns); L5 (50 ns); F33 (106 ns)	

[a]Only the insertions of large hydrophobic residues (Phe, Trp, Met, Leu, and Ile) are considered.

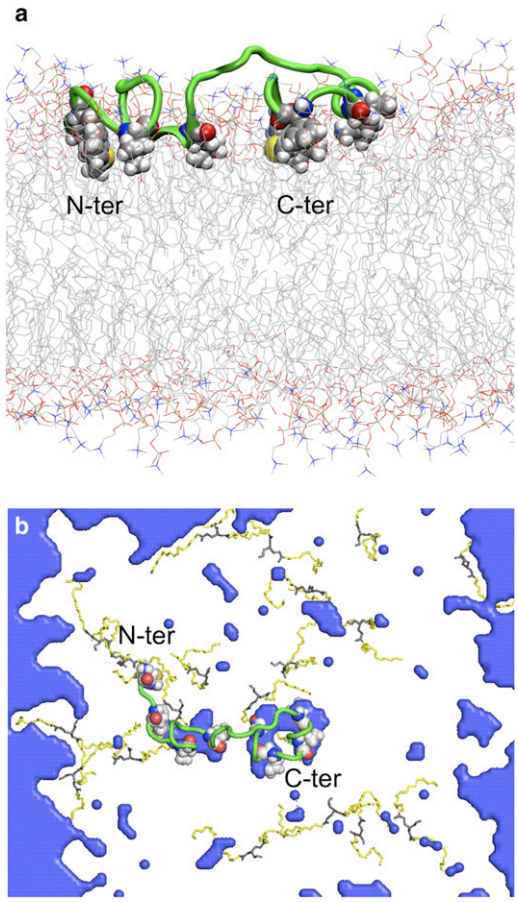

FIGURE 6 The ALPS motif of GMAP210 exhibits repeated hydrophobic insertions in DOPC/DOG bilayers. (*a*) Side view of an MD snapshot (after 1 μs) of the ALPS motif of GMAP210 inserted into a DOPC/DOG lipid bilayer. The peptide is shown in green in cartoon representation and the inserting hydrophobic residues (M1, W4, L5, L8, L16, L26, I30, F33, M37, and L38) are shown in vdW representation. (*b*) Top view of the colocalization between the hydrophobic insertions and geometrical lipid packing defects (*blue*). DOG molecules are shown in licorice representation. C- and N-terminal regions are explicitly indicated. A small defect below the N-terminus is not visible due to overlap with the N-terminus of the peptide.

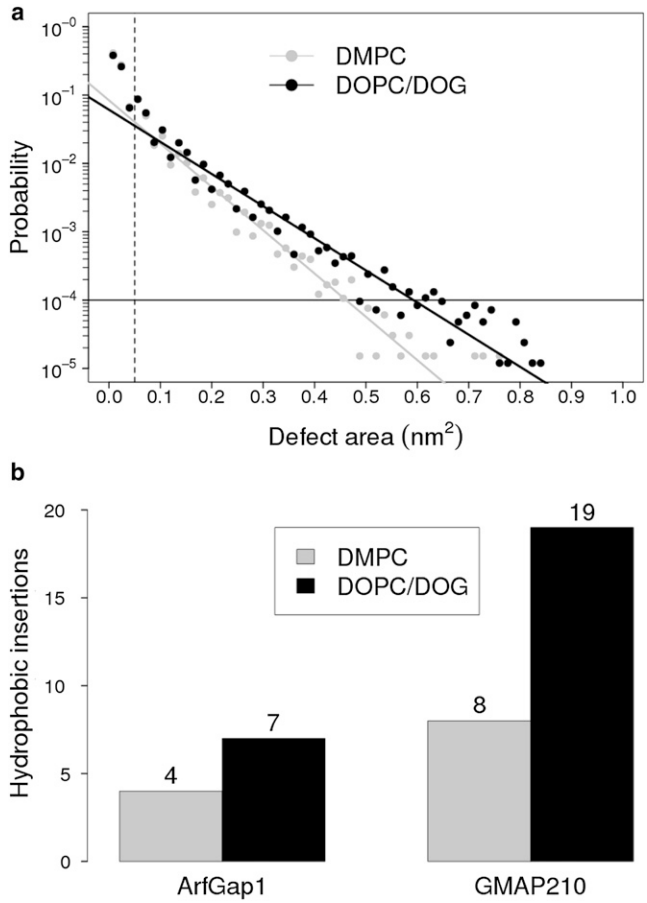

FIGURE 7 Effect of packing defects on ALPS partitioning in the lipid bilayer. (*a*) Size distribution of packing defects for mixed DOPC/DOG (*black*) and pure DMPC (*gray*) bilayers. The ratio between the total area of lipid packing defects > 0.2 nm^2 and the total surface area is 0.47% for DOPC/DOG and 0.19% for DMPC. (*b*) Total number of hydrophobic insertions in five independent MD simulations of 400 ns each for the ALPS motifs of ArfGAP1 and GMAP210 with DOPC/DOG (*black*) and DMPC (*gray*) bilayers. (Note that panel *a* is a simplified version of Fig. 5 in the companion article (23).

protocol (see Materials and Methods). The data presented in Fig. 7 *b* were collected from five MD replicas of 400 ns each in the following systems: ArfGAP1+DOPC/DOG, ArfGAP1+DMPC, GMAP210+DOPC/DOG, and GMAP210+DMPC (see Table 2 for additional details).

The data shown in Fig. 7 *b* support the notion that the statistical distribution of packing defects is a critical feature of ALPS binding to model membranes. In particular, although the molecular mechanism of partitioning is the same, the total number of hydrophobic insertions of ALPS motifs decreased substantially from DOPC/DOG to DMPC. A similar behavior was observed for both the toluene molecules and the model peptide SLG (see Supporting Material).

The average depth of insertion also appeared to be more pronounced in the DOPC/DOG bilayer, but the limited number of insertions observed in the case of DMPC did not allow us to obtain a reliable estimate for this property. In addition, whereas in the case of DOPC/DOG the peptides always bound to the lipid bilayer, this was not the case for DMPC. Indeed, three out of the 10 simulations of ALPS motifs in the presence of a DMPC bilayer did not show any insertion event in the first 400 ns (Table 2).

Finally, it must be noted that the ratio between hydrophobic insertions in DOPC/DOG versus DMPC bilayers is more pronounced in the MD simulations of GMAP210 than in those of ArfGAP1. This is not unexpected if the probability of hydrophobic insertion is proportional to the likelihood of detecting a packing defect of a given size. Because it partitions into the bilayer more rapidly than the ALPS motif of ArfGAP1, the GMAP210 ALPS motif is more suited to detect differences between the two bilayers within the timescales of our computational technique.

CONCLUSIONS

Because of their sensitivity to membrane curvature and to the insertion of conical lipids in flat bilayers, ALPS motifs have been defined as lipid-packing sensors (10). However, the concept of lipid packing defects is inherently microscopic, and its explicit characterization with biophysical experiments has not been possible so far.

Atomistic MD simulations indicate that packing defects are indeed a measurable geometrical property of membranes, and that bilayers of different curvature (22) and/or composition (23) display different packing defect structures that one can identify by plotting their occurrence against their size. Importantly, the main differences between bilayers occur for packing defects of large size.

In a previous study, we examined the behavior of the ALPS motif of ArfGAP1 when it was folded in its α-helical conformation and embedded inside a DOPC/DOG membrane (17). In this work, we performed MD simulations of ALPS motifs in the presence of lipid bilayers to examine the early steps of binding and to understand the relationship between packing defects and the mechanism of membrane curvature sensing by ALPS motifs. With this technique, we are limited to timescales of the order of the microsecond and cannot follow the complete partitioning and folding of the peptide at physiological temperature. Nevertheless, we could repeatedly observe spontaneous hydrophobic insertions in the bilayer with very high resolution and collect enough sampling to correlate peptide binding with the behavior of packing defects in model membranes.

Our results indicate that packing defects are equivalent to nonspecific dynamical binding pockets for membrane sensor peptides, and that ALPS motifs bind to large preexisting packing defects. The overall process of adsorption proceeds through separate insertions of bulky hydrophobic residues below the glycerol level. Remarkably, the fact that we were able to tune the occurrence probability of large packing defects either by introducing conical lipids or by altering the number of monounsaturated acyl chains composing our bilayer implies that a well-localized interfacial event, such as binding of a peripheral protein, can be controlled by bulk properties of the bilayer in a nontrivial way.

Besides ALPS motifs, other protein modules use hydrophobic residues or modifications to bind to lipid membranes. Therefore, and as previously proposed (7,19), sensing of membrane curvature through the detection of packing defects may be a quite general mechanism. However, in other molecular contexts (e.g., BAR domains and α-synuclein), hydrophobic insertions of various sizes combine with other mechanisms, such as electrostatics or scaffolding (20,43–46), thereby obscuring the role of lipid packing defects in the overall process of membrane binding.

What is remarkable in the case of ALPS motifs is the exclusive use of hydrophobic insertions all along their sequence. This specificity amplifies the role of packing defects in the mechanism of peptide binding and can be appreciated by comparing an elementary insertion event in a DMPC bilayer and a DOPC/DOG bilayer, two extreme cases in terms of lipid packing defect distributions. In both cases, a packing defect large enough to accommodate the insertion of a first hydrophobic residue can be found. However, the scarcity of large lipid packing defects in the DMPC membrane makes this event less likely. Thereafter, the ALPS motif, which is quite flexible owing to its glycine residues, may detect packing defects that are spatially distant from the first one. Therefore, the second insertion should be governed by the same probability function as the first one, and should be less favorable in a DMPC membrane than in a DOPC/DOG membrane. On the scale of a complete ALPS motif containing five to 10 putative hydrophobic insertions, this iterative process, which is analogous to probing n times the packing structure of the bilayer (4), should result in a dramatic increase in sensitivity. Even if other energetic terms (e.g., the contributions arising from peptide folding and lipid rearrangements) are likely to contribute to the overall thermodynamic behavior of the system, the mechanism highlighted by the MD simulations helps us understand how ALPS motifs are able to trigger biochemical pathways by responding so effectively to small differences in lipid packing that arise from modest changes in the molecular architecture of the cell (e.g., when the radius of a Golgi vesicle changes from 60 to 30 nm).

SUPPORTING MATERIAL

Six supplemental figures, one table, and reference (47) are available at http://www.biophysj.org/biophysj/supplemental/S0006-3495(12)05143-0.

The authors thank Luca Monticelli for providing the initial topology of DOPC lipids, Drew Bennett and Peter Tieleman for the force field of toluene, all members of the Antonny laboratory for support and comments, and Alenka Copic for comments on the manuscript.

This work used the high-performance computing resources of CINES under allocations c2011-076720, c2012-076720, and c2012-076859 from Grand Equipement National de Calcul Intensif. Some computations were done on the Mesocentre SIGAMM machine hosted by the Observatoire de la Cote d'Azur. This work was supported by the Swiss National Science Foundation (grant PBELP3_141118 to S.V.), the French Government (grant MENRT to L.V.), and the European Research Council (advanced grant 268888 to B.A.).

REFERENCES

1. Antonny, B., I. Huber, …, D. Cassel. 1997. Activation of ADP-ribosylation factor 1 GTPase-activating protein by phosphatidylcholine-derived diacylglycerols. *J. Biol. Chem.* 272:30848–30851.

2. Bigay, J., P. Gounon, …, B. Antonny. 2003. Lipid packing sensed by ArfGAP1 couples COPI coat disassembly to membrane bilayer curvature. *Nature*. 426:563–566.

3. McMahon, H. T., and J. L. Gallop. 2005. Membrane curvature and mechanisms of dynamic cell membrane remodelling. *Nature*. 438: 590–596.

4. Antonny, B. 2011. Mechanisms of membrane curvature sensing. *Annu. Rev. Biochem.* 80:101–123.
5. Zimmerberg, J., and M. M. Kozlov. 2006. How proteins produce cellular membrane curvature. *Nat. Rev. Mol. Cell Biol.* 7:9–19.
6. Roux, A., G. Koster, …, P. Bassereau. 2010. Membrane curvature controls dynamin polymerization. *Proc. Natl. Acad. Sci. USA.* 107: 4141–4146.
7. Bhatia, V. K., N. S. Hatzakis, and D. Stamou. 2010. A unifying mechanism accounts for sensing of membrane curvature by BAR domains, amphipathic helices and membrane-anchored proteins. *Semin. Cell Dev. Biol.* 21:381–390.
8. Rudner, D. Z., and R. Losick. 2010. Protein subcellular localization in bacteria. *Cold Spring Harb. Perspect. Biol.* 2:a000307.
9. Drin, G., V. Morello, …, B. Antonny. 2008. Asymmetric tethering of flat and curved lipid membranes by a golgin. *Science.* 320:670–673.
10. Bigay, J., J. F. Casella, …, B. Antonny. 2005. ArfGAP1 responds to membrane curvature through the folding of a lipid packing sensor motif. *EMBO J.* 24:2244–2253.
11. Drin, G., J. F. Casella, …, B. Antonny. 2007. A general amphipathic α-helical motif for sensing membrane curvature. *Nat. Struct. Mol. Biol.* 14:138–146.
12. Doucet, C. M., J. A. Talamas, and M. W. Hetzer. 2010. Cell cycle-dependent differences in nuclear pore complex assembly in metazoa. *Cell.* 141:1030–1041.
13. Cabrera, M., L. Langemeyer, …, C. Ungermann. 2010. Phosphorylation of a membrane curvature-sensing motif switches function of the HOPS subunit Vps41 in membrane tethering. *J. Cell Biol.* 191:845–859.
14. Krabben, L., A. Fassio, …, V. Haucke. 2011. Synapsin I senses membrane curvature by an amphipathic lipid packing sensor motif. *J. Neurosci.* 31:18149–18154.
15. Fan, W., A. Nassiri, and Q. Zhong. 2011. Autophagosome targeting and membrane curvature sensing by Barkor/Atg14(L). *Proc. Natl. Acad. Sci. USA.* 108:7769–7774.
16. Mesmin, B., G. Drin, …, B. Antonny. 2007. Two lipid-packing sensor motifs contribute to the sensitivity of ArfGAP1 to membrane curvature. *Biochemistry.* 46:1779–1790.
17. González-Rubio, P., R. Gautier, …, P. F. Fuchs. 2011. Amphipathic-Lipid-Packing-Sensor interactions with lipids assessed by atomistic molecular dynamics. *Biochim. Biophys. Acta.* 1808:2119–2127.
18. Baumgart, T., B. R. Capraro, …, S. L. Das. 2011. Thermodynamics and mechanics of membrane curvature generation and sensing by proteins and lipids. *Annu. Rev. Phys. Chem.* 62:483–506.
19. Hatzakis, N. S., V. K. Bhatia, …, D. Stamou. 2009. How curved membranes recruit amphipathic helices and protein anchoring motifs. *Nat. Chem. Biol.* 5:835–841.
20. Bartels, T., L. S. Ahlstrom, …, K. Beyer. 2010. The N-terminus of the intrinsically disordered protein α-synuclein triggers membrane binding and helix folding. *Biophys. J.* 99:2116–2124.
21. Lee, A. G. 2004. How lipids affect the activities of integral membrane proteins. *Biochim. Biophys. Acta.* 1666:62–87.
22. Cui, H., E. Lyman, and G. A. Voth. 2011. Mechanism of membrane curvature sensing by amphipathic helix containing proteins. *Biophys. J.* 100:1271–1279.
23. Vamparys, L., R. Gautier, …, P. F. J. Fuchs. 2013. Conical lipids in flat bilayers induce packing defects similar to that induced by positive curvature. *Biophys. J.* 104:585–593.
24. Hess, B., C. Kutzner, …, E. Lindahl. 2008. GROMACS 4: algorithms for highly efficient, load-balanced, and scalable molecular dynamics simulation. *J. Chem. Theory Comput.* 4:435–447.
25. Jorgensen, W. L., D. S. Maxwell, and J. Tirado-Rives. 1996. Development and testing of the OPLS All-atom force field on conformational energetics and properties of organic liquids. *J. Am. Chem. Soc.* 118:11225–11236.
26. Tieleman, D. P., J. L. Maccallum, …, L. Monticelli. 2006. Membrane protein simulations with a united-atom lipid and all-atom protein model: lipid-protein interactions, side chain transfer free energies and model proteins. *J. Phys. Condens. Matter.* 18:S1221–S1234.
27. Berger, O., O. Edholm, and F. Jähnig. 1997. Molecular dynamics simulations of a fluid bilayer of dipalmitoylphosphatidylcholine at full hydration, constant pressure, and constant temperature. *Biophys. J.* 72:2002–2013.
28. Jorgensen, W. L., W. L. Jorgensen, …, M. L. Klein. 1983. Comparison of simple potential functions for simulating liquid water. *J. Chem. Phys.* 79:926–935.
29. Chakrabarti, N., C. Neale, …, R. Pomès. 2010. An iris-like mechanism of pore dilation in the CorA magnesium transport system. *Biophys. J.* 98:784–792.
30. Essmann, U., L. Perera, …, L. G. Pedersen. 1995. A smooth particle mesh ewald method. *J. Chem. Phys.* 103:8577–8593.
31. Hess, B., H. Bekker, …, J. G. E. M. Fraaije. 1997. LINCS: a linear constraint solver for molecular simulations. *J. Comput. Chem.* 18: 1463–1472.
32. Bussi, G., D. Donadio, and M. Parrinello. 2007. Canonical sampling through velocity rescaling. *J. Chem. Phys.* 126:014101.
33. Parrinello, M., and A. Rahman. 1981. Polymorphic transitions in single-crystals—a new molecular-dynamics method. *J. Appl. Phys.* 52:7182–7190.
34. MacCallum, J. L., W. F. Bennett, and D. P. Tieleman. 2008. Distribution of amino acids in a lipid bilayer from computer simulations. *Biophys. J.* 94:3393–3404.
35. Humphrey, W., A. Dalke, and K. Schulten. 1996. VMD: visual molecular dynamics. *J. Mol. Graph.* 14:33–38, 27–28.
36. DeLano, W. L. The PyMOL molecular graphics system. DeLano Scientific LLC, San Carlos, CA. http://www.pymol.org.
37. Ladokhin, A. S., and S. H. White. 1999. Folding of amphipathic α-helices on membranes: energetics of helix formation by melittin. *J. Mol. Biol.* 285:1363–1369.
38. White, S. H., and W. C. Wimley. 1998. Hydrophobic interactions of peptides with membrane interfaces. *Biochim. Biophys. Acta.* 1376: 339–352.
39. Ulmschneider, M. B., J. P. Doux, …, J. P. Ulmschneider. 2010. Mechanism and kinetics of peptide partitioning into membranes from all-atom simulations of thermostable peptides. *J. Am. Chem. Soc.* 132:3452–3460.
40. Tang, J., R. S. Signarvic, …, F. Gai. 2007. Role of helix nucleation in the kinetics of binding of mastoparan X to phospholipid bilayers. *Biochemistry.* 46:13856–13863.
41. Zasloff, M. 2002. Antimicrobial peptides of multicellular organisms. *Nature.* 415:389–395.
42. Wang, Y., D. E. Schlamadinger, …, J. A. McCammon. 2012. Comparative molecular dynamics simulations of the antimicrobial peptide CM15 in model lipid bilayers. *Biochim. Biophys. Acta.* 1818:1402–1409.
43. Pranke, I. M., V. Morello, …, C. L. Jackson. 2011. α-Synuclein and ALPS motifs are membrane curvature sensors whose contrasting chemistry mediates selective vesicle binding. *J. Cell Biol.* 194:89–103.
44. Cui, H., G. S. Ayton, and G. A. Voth. 2009. Membrane binding by the endophilin N-BAR domain. *Biophys. J.* 97:2746–2753.
45. Arkhipov, A., Y. Yin, and K. Schulten. 2009. Membrane-bending mechanism of amphiphysin N-BAR domains. *Biophys. J.* 97:2727–2735.
46. Taylor, A., and M. S. Sansom. 2010. Studies on viral fusion peptides: the distribution of lipophilic and electrostatic potential over the peptide determines the angle of insertion into a membrane. *Eur. Biophys. J.* 39:1537–1545.
47. Berendsen, H. J. C., J. P. M. Postma, …, J. R. Haak. 1984. Molecular-dynamics with coupling to an external bath. *J. Chem. Phys.* 81:3684–3690.